ACS OMEGA

http://pubs.acs.org/journal/acsodf

Article

The Role of Some Cationic Surfactants Based on Thiazine as Corrosion Inhibitors in Petroleum Applications: Experimental and Theoretical Approach

Mohamed A. Moselhy, Elsayed Gamal Zaki,* Samir Abd El Hady Abd El-Maksoud, and Mohamed A. Migahed

Cite This: *ACS Omega* 2022, 7, 32014−32025

Read Online

ACCESS | Metrics & More | Article Recommendations

ABSTRACT: Two cationic surfactants based on thiazine, dodecyl thiazin bromide (DTB) and hexyl thiazin bromide (HTB), were synthesized, characterized, and investigated as corrosion inhibitors for API X-65 type steel in oil wells' formation water under an H_2S environment. Various spectroscopic techniques such as FTIR and ^1H NMR were used to confirm the DTB and HTB chemical structures. The corrosion inhibition efficiency of the selected compounds was investigated using both potentiodynamic polarization and electrochemical impedance spectroscopy (EIS) measurements. The innovation of the current study is the existence of a long chain in the inhibitor molecule, which leads to an increase in the performance of the surfactant as a corrosion inhibitor, due to the increase in the surface area per molecule. It was found that these surfactants act as mixed-type inhibitors, leading to suppression of both the cathodic and the anodic processes by its adsorption on the electrode surface according to the Langmuir adsorption isotherm. Carbon steel's inhibitory mechanism was studied using an analogous circuit. The scanning electron microscope technique was used as a suitable analysis tool to show the nature of the layer designed on carbon steel. Quantum chemical calculations and Monte Carlo simulation techniques were used to support the obtained experimental results. Finally, a suitable mechanism for the inhibition process was proposed and discussed.

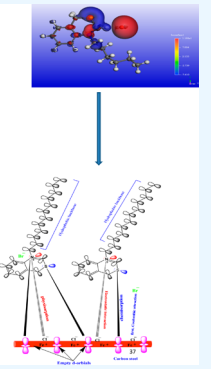

1. INTRODUCTION

Carbon steel is commonly used in petroleum processing facilities for refining and marine applications, due to its mechanical properties and also from an economical point of view.[1,2] It is well-known that the metallic surfaces are suffering from corrosion, and this is leading to significant economic losses in addition to a bad environmental impact.[3,4] It was reported in the literature that organic compounds with hetero atoms such as nitrogen, oxygen, sulfur, and phosphorus show promising efficiency in mitigating the aggressive attack of corrosive species on a metal surface.[5,6] These types of organic compounds act at the interface between the metal and the aggressive solution through the adsorption on metal surfaces, forming a protective layer that isolates the metallic surfaces from the corrosive environment.[7] Accordingly, the selection of this type of cationic surfactants in the present work is attributed to the presence of incorporated hetero-organic moieties, which offer more protection potential against the corrosion of steel, along with the presence of a long chain that increases the minimum area per molecule.[8−13] Cationic surfactants are a category of surface-active agents that dissociate in water to create surface-active cations. Because of the beneficial characteristics of these cationic surfactants, they have numerous applications in many sectors. It was reported that they are adsorbed on metal surfaces by both physical and chemical methods.[14−18] The novelty of the present work appears in using cationic surfactants containing a long chain and heteroatoms as nitrogen and sulfur, besides for the high solubility in oil wells' formation water contaminated with H_2S gas. The present work is aimed to prepare two novel cationic surfactants, DTB and HTB, and evaluate their performance as corrosion inhibitors for carbon steel in formation water under an H_2S environment using different techniques. Also, our work is extended to carry out some theoretical studies to support the obtained experimental results. This Article is regarded as an onset of a series of works currently under investigation in our lab.

2. RESULTS AND DISCUSSION

2.1. Potentiodynamic Polarization Measurements.

Iron dissolution results in ferrous sulfide as the primary corrosion product when H_2S is present; however, the protective layer is dissolved when the H_2S gas concentration is high. The electrochemical parameters including the

Received: May 14, 2022
Accepted: August 17, 2022
Published: August 31, 2022

Table 1. Polarization Parameters of the CS at Various Concentrations of DTB and HTB in Formation Water and the Corresponding Inhibition Efficiencies

inhibitor	concn (ppm)	β_a, (mV dec^{-1})	$-\beta_c$, (mV dec^{-1})	$-E_{corr}$ (mV vs SCE)	I_{corr}, (μA cm^{-2})	θ	IE%
blank	0	193.7 ± 1.2	150.9 ± 1.3	828.3 ± 7.2	9.31 ± 0.02		
DTB	50	112.8 ± 1.3	155.3 ± 1.4	800.1 ± 5.6	3.71 ± 0.01	0.6015	60.15
	100	108.3 ± 1.7	142.5 ± 1.5	814.2 ± 4.3	2.92 ± 0.01	0.6863	68.63
	150	102.7 ± 1.9	139.7 ± 1.6	764.5 ± 3.1	1.85 ± 0.01	0.8012	80.12
	200	99.1 ± 2.1	136.1 ± 1.9	780.4 ± 2.6	1.37 ± 0.01	0.8528	85.28
	250	95.6 ± 2.3	135.4 ± 2.1	716.2 ± 2.5	0.97 ± 0.01	0.92058	92.058
HTB	50	109.2 ± 1.5	166.7 ± 1.5	776.4 ± 6.8	3.97 ± 0.01	0.5735	57.35
	100	107.6 ± 1.9	145.2 ± 1.7	814.1 ± 3.9	3.35 ± 0.01	0.6401	64.01
	150	103.8 ± 2.3	140.8 ± 1.9	788.5 ± 2.8	2.15 ± 0.01	0.7690	76.90
	200	101.5 ± 2.4	138.3 ± 2.1	740.2 ± 5.4	1.76 ± 0.01	0.8109	81.09
	250	100.8 ± 1.9	136.1 ± 2.3	722.6 ± 1.9	1.24 ± 0.01	0.8668	86.68

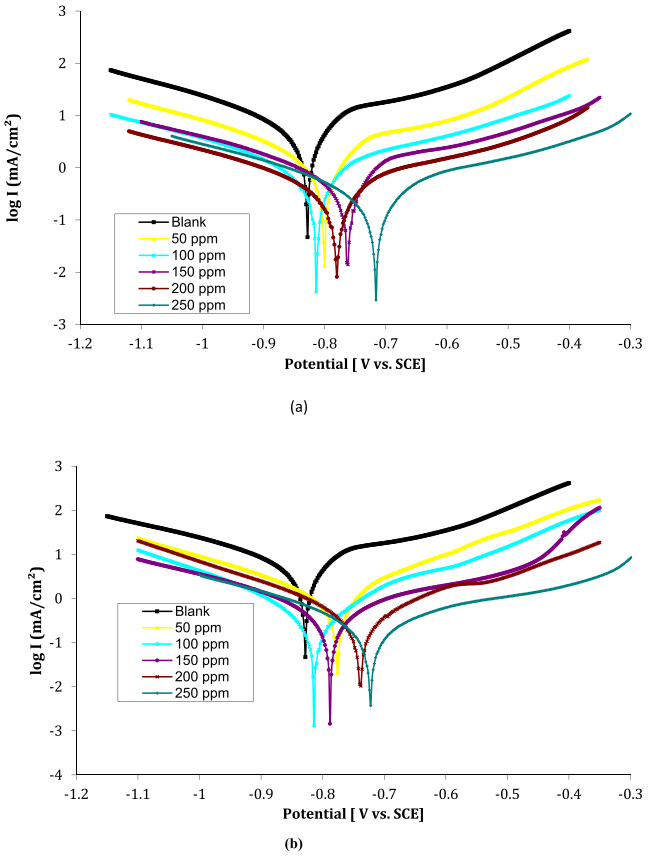

Figure 1. Potential−log current density curves of carbon steel electrode immersed in formation water in the absence and presence of different doses of (a) DTB and (b) HTB inhibitors.

corrosion current density (i_{corr}), the corrosion potential (E_{corr}), the anodic and cathodic Tafel slopes (β_a and β_c), the degree of surface coverage, and the percentage inhibition efficiency were calculated[19−26] and are tabulated in Table 1.

Figure 1a,b shows the polarization curves of the two compounds DTB and HTB with respect to the blank curve. By careful inspection of the polarization curves, it is clear that the values of the corrosion current density (i_{corr}) were significantly reduced by increasing the dose of chemical injected. The values of inhibition efficiency (η%) and the degree of surface coverage (θ) were calculated according to the following equations:

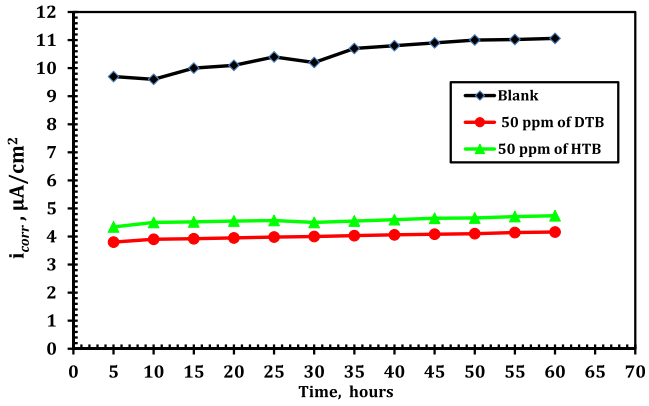

Figure 2. The variation of corrosion current density with the immersion time for carbon steel in formation water in the absence and presence of 50 ppm of the inhibitors (DTB and HTB).

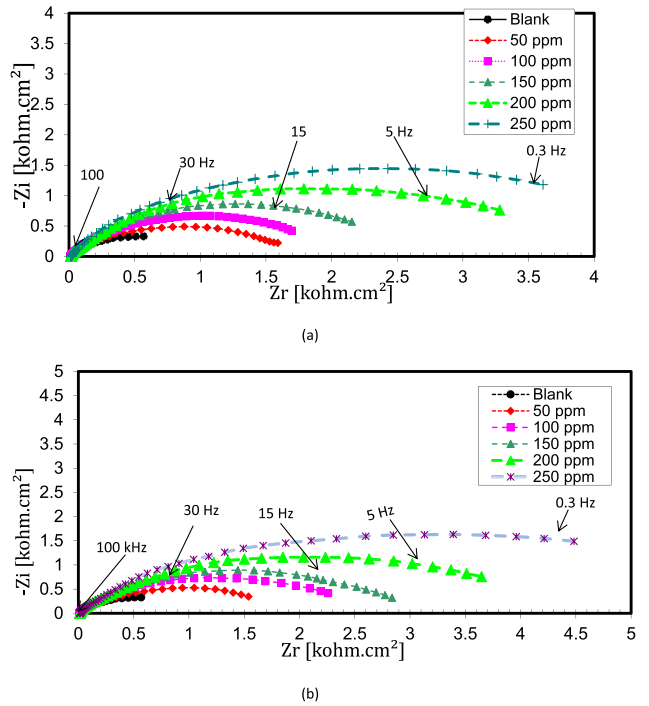

Figure 3. EIS data (Nyquist plots) for carbon steel immersed in oil field formation water in the presence and absence of various doses of (a) DTB and (b) HTB.

https://doi.org/10.1021/acsomega.2c02961
ACS Omega 2022, 7, 32014−32025

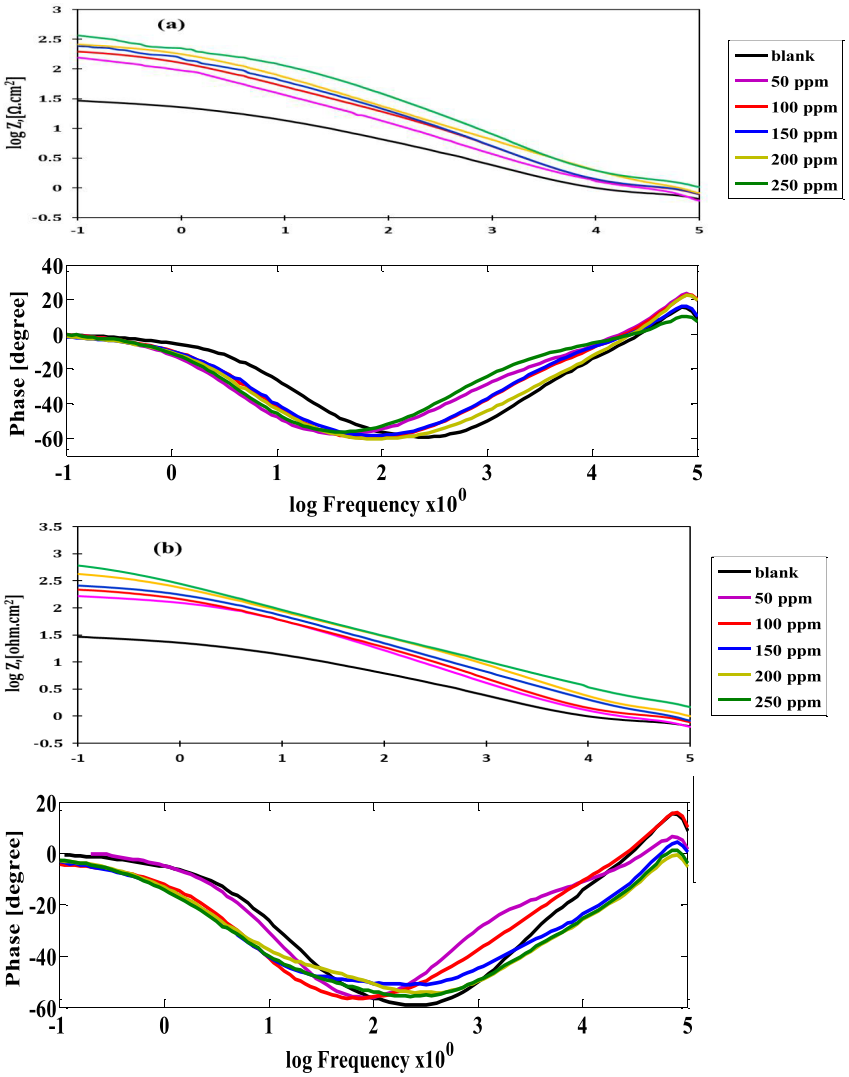

Figure 4. EIS data (Bode plots) for carbon steel immersed in oil field formation water in the presence and absence of various doses of (a) DTB and (b) HTB.

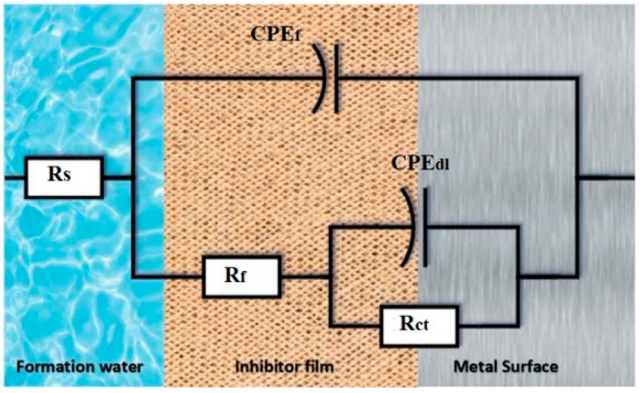

Figure 5. EIS data for CS in the used formation water modeled using an equivalent circuit.

$$\theta = 1 - \frac{i}{i_0} \quad (1)$$

$$\eta\,\% = \left(1 - \frac{i}{i_0}\right) \quad (2)$$

where i and i_0 represent the values of the corrosion current densities in the presence and absence of various doses of the inhibitor, respectively.

A careful inspection of the polarization curves indicated that the Tafel lines of the two compounds (DHB and HTB) are slightly shifted to more positive potentials with respect to the blank. This fact means that the organic compounds under consideration work as a mixed type; that is, they retard both anodic dissolution of carbon steel in addition to the cathodic discharge reaction. Also, it is clear that the values of both β_a and β_c are nearly constant and do not depend on the change in inhibitor concentrations. This behavior confirms that inhibitors under investigation retard the corrosion process with a change in the mechanism of occurrence. The corrosion current densities (i_{corr}) decreased with increasing concentration.[27] The obtained results in Table 1 indicated that the corrosion current density values are significantly lower in the presence of the corrosion inhibitors as compared to the uninhibited solution.

The results show that compound DTB has a better percentage inhibition efficiency than that of compound HTB. The p−d bonds can be formed between inhibitor molecules and the empty orbital of iron, which may explain this.[28−30]

https://doi.org/10.1021/acsomega.2c02961
ACS Omega 2022, 7, 32014−32025

Table 2. Impedance Parameters Obtained from EIS curves for the DTB and HTB Inhibitors

inhibitor	concn (ppm)	n_1	R_f	Q_F	n_2	Q_{dl} (μF/cm^2)	R_{ct}	θ	IE%
DTB	0	0.87 ± 0.02	52.6 ± 2.1	132.1 ± 1.1	0.83 ± 0.05	538.1 ± 1.1	1.659 ± 0.10		
	50	0.90 ± 0.03	12.3 ± 4.3	83.9 ± 0.8	0.87 ± 0.04	138.7 ± 3.5	2.81 ± 0.19	0.4132	41.32
	100	0.92 ± 0.02	2.77 ± 6.5	57.4 ± 0.6	0.89 ± 0.02	117.2 ± 3.9	3.73 ± 0.23	0.5581	55.81
	150	0.94 ± 0.01	3.9 ± 8.3	48.5 ± 0.5	0.91 ± 0.01	116.5 ± 4.3	4.51 ± 0.27	0.6347	63.47
	200	0.95 ± 0.01	527 ± 9.1	39.2 ± 0.4	0.92 ± 0.08	104.3 ± 5.7	8.66 ± 0.33	0.8095	80.95
	250	0.96 ± 0.01	544 ± 4.5	34.7 ± 0.6	0.93 ± 0.07	89.4 ± 6.2	13.31 ± 0.42	0.8761	87.61
HTB	50	0.89 ± 0.03	118 ± 3.5	79.3 ± 0.9	0.85 ± 0.2	132.6 ± 3.3	2.67 ± 0.17	0.3821	38.21
	100	0.91 ± 0.04	253 ± 6.3	62.8 ± 0.7	0.87 ± 0.01	113.4 ± 3.8	3.28 ± 0.21	0.4983	49.83
	150	0.92 ± 0.06	297 ± 7.1	38.5 ± 0.6	0.88 ± 0.02	97.3 ± 4.1	4.29 ± 0.25	0.6158	61.58
	200	0.93 ± 0.07	463 ± 8.3	29.1 ± 0.5	0.89 ± 0.03	93.2 ± 5.3	7.71 ± 0.31	0.7862	78.62
	250	0.94 ± 0.06	492 ± 9.1	19.2 ± 0.4	0.91 ± 0.03	85.1 ± 5.7	10.96 ± 0.39	0.8411	84.11

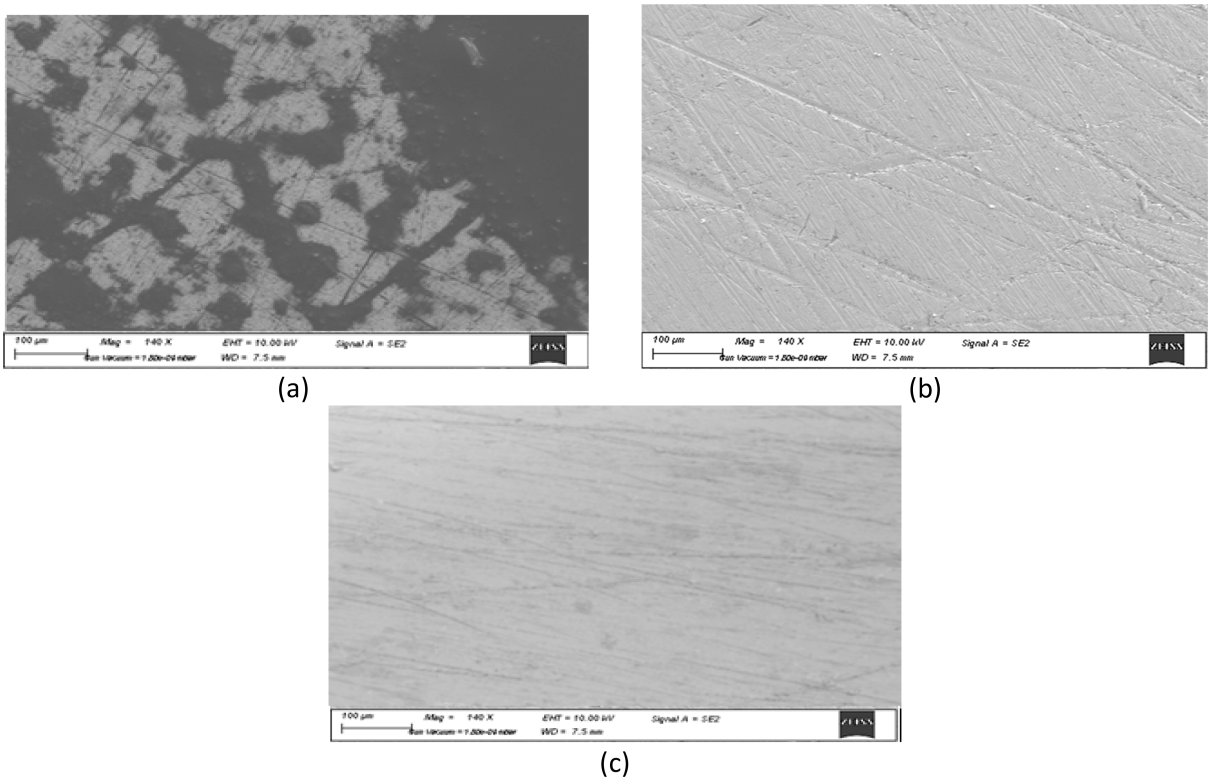

Figure 6. SEM analysis for the X-65 carbon steel surface. Sample (a) after immersion in test solution, (b) after immersion in test solution containing 250 ppm of DTB, and (c) after immersion in test solution containing 250 ppm of HTB.

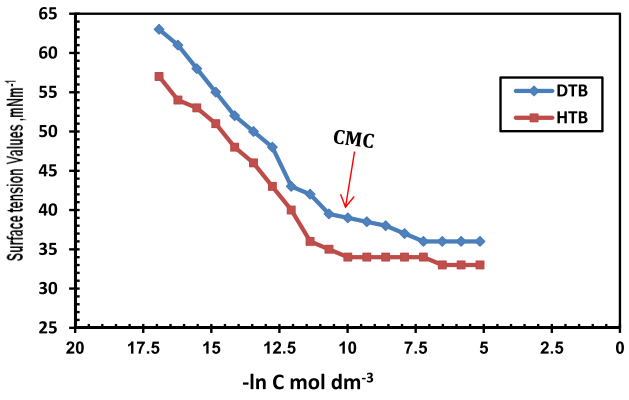

Figure 7. Surface tension versus ln C of the compounds DTB and HTB.

This could be attributed to the increase leading to an increase in the surface area per molecule that covers the surface of carbon steel and isolates it from the aggressive environment.

The long-term behavior of the undertaken compounds (DTB and HTB) as corrosion inhibitors was studied by plotting the corrosion current density (i_{corr}) against the immersion time (t) as shown in Figure 2. It is clear from the change in i_{corr} with time that the undertaken compounds (DTB and HTB) were adsorbed on the carbon steel surface to form a stable protective film for a long period of time.

2.2. Electrochemical Impedance Spectroscopy (EIS). Nyquist and Bode plots of carbon steel in oil field formation water in the absence and presence of various doses of the compounds DTB and HTB are shown in Figures 3 and 4, respectively.

By careful inspection of Figure 4, one can conclude that the size of the obtained capacitive loop along the x-axis was increased with increasing concentrations of the two inhibitors

https://doi.org/10.1021/acsomega.2c02961
ACS Omega 2022, 7, 32014−32025

Table 3. Surface Active Properties of the Synthesized Compounds DTB and HTB

inhibitor concn	CMC, mol/dm^3	γ_{cmc}, mN/m	$\Gamma_{max} \times 10^{-7}$, mol/m^2	$A_{min,n}$, m^2	Π_{CMC}	ΔG_{mic}°, kJ mol^{-1}	ΔG_{ads}°, kJ mol^{-1}
DTB	2.49×10^{-5}	35	9.72×10^{-11}	170	37.3	−26.70	−30.35
HTB	1.84×10^{-4}	33	6.65×10^{-10}	191	39.3	−21.66	−26.20

Table 4. Standard Free Energy of Micellization (ΔG_{mic}°) and Standard Free Energy of Adsorption (ΔG_{ads}°) as Obtained from Surface Tension Measurements and the Langmuir Adsorption Isotherm Model, Respectively

inhibitor	free energy of micellization, ΔG_{mic}° (kJ mol^{-1})	free energy of adsorption, ΔG_{ads}° (kJ mol^{-1})
DTB	−26.70	−30.35
HTB	−21.66	−26.20

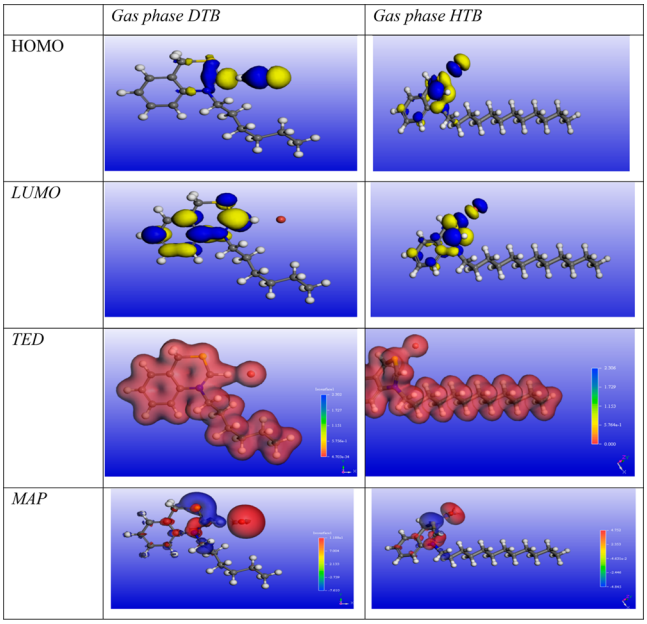

Figure 8. Optimized molecular structures, HOMO, LUMO, total electron density distribution, and MAP, of DTB and HTB in the gas phase.

under investigation, that is, DTB and HTB. From this behavior, it is evident that both the corrosion and the inhibition processes were controlled by the value of polarization resistance R_p according to the following equation:

$$R_p = R_s + R_f + R_{ct} \quad (3)$$

Figure 5 shows in detail the equivalent circuit that fit well the obtained data where the solution resistance is R_s, film resistance is R_f, charge transfer resistance is R_{ct}, and constant phase elements are CPE_F and CPE_{dl}. The acquired impedance data can be described by the equation below, as derived by the EIS analyzer program.

$$Z_{cpe} = 1 / Y_0(jw)^n \quad (4)$$

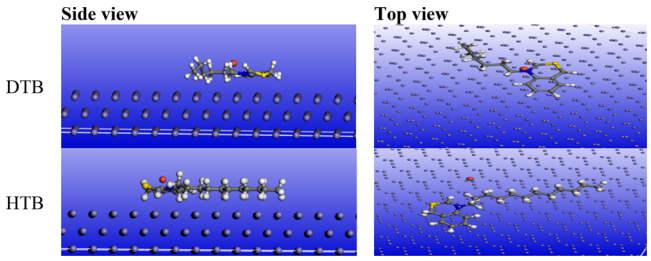

Figure 9. Side and top views of the adsorption mode of DTB and HTB on Fe (110) substrate.

where Y_0 represents the admittance, $j = -1$, and w is the angular frequency.

Table 2 clearly shows that as the DTB and HTB concentrations rise, both C_{dl} and C_f drop. Molecular inhibitor adsorption to the necessary protective layer on carbon steel surfaces is indicated by this finding. According to the following two equations:[31]

$$C_{dl} = \Sigma^0 \Sigma Se / d \quad (5)$$

$$C_f = F^2 Se / 4RT \quad (6)$$

$\sum^0$ is the electrode surface exposed to the aggressive solution with a permittivity of 0, and this is determined by the adsorbed layer thickness (d), $\sum$ is the local dielectric constant, and F is the Faraday constant. Also, it is clear from the Bode plots in Figure 4 that both phase angle and absolute impedance are increased by increasing the inhibitor concentrations. Such behavior supports well the inhibition effect of the selected compounds (DTB and HTB).[32−35]

2.3. SEM Examination. SEM photomicrograph analysis is considered a powerful tool to observe the change in surface morphology of the investigated alloy, that is, X-65 type, dipped in the oil well water after and before adding inhibitor for 15 days. Figure 6a shows the SEM image for a specimen of carbon steel immersed in the oil formation water without inhibitor (blank). It is clear that the surface is thoroughly damaged due to the presence of aggressive ions that attack on the surface, leading to Sevier corrosion. Figure 6b shows the SEM image for a specimen of carbon steel immersed in the oil formation water in the presence of 250 ppm of the inhibitor DTB, while Figure 6c shows the SEM image for a specimen of carbon steel immersed in the oil formation water in the presence of 250 ppm of the inhibitor HTB. The above features confirm the anticorrosion behavior of the prepared compounds for X-65 steel in the formation water, which well agrees with other electrochemical results.

2.4. Surface Tension Measurements. The CMC values of the synthesized surfactants were determined at various

Table 5. Quantum Chemical Parameters of the Investigated Inhibitor

	E_H (eV)	E_L (eV)	ΔE_{gap}	A	I	χ	η	ΔN
DTB	−8.386	−1.606	6.78	1.606	8.386	4.996	3.39	0.295575221
HTB	−7.908	−1.089	6.819	1.089	7.908	4.4985	3.4095	0.366842646

https://doi.org/10.1021/acsomega.2c02961
ACS Omega 2022, 7, 32014−32025

Table 6. Output Energies Calculated by Monte Carlo Simulation for DTB and HTB in the Gas Phase on Fe (110)

parameters	total energy	adsorption energy	rigid adsorption energy	deformation energy	3D atomistic
DTB	−157.11	−434.47	−137.99	−296.47	−434.47
HTB	−229.70	−552.68	−198.41	−354.27	−552.68

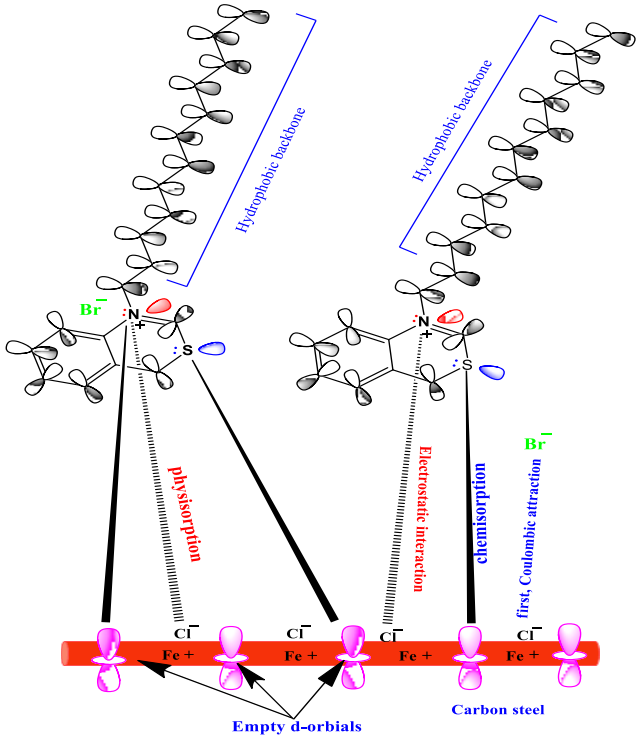

Figure 10. Mechanism of the corrosion inhibition of DTB.

temperatures from the change in the slope of the plotted data of surface tension (γ) versus the natural logarithm of the solute molar concentration, ln C, as shown in Figure 7. The surface active properties obtained from the surface tension measurements are summarized and listed in Table 3.

The properties of the surfactant molecules are due to two parts: the organic hydrophobic part and the polar hydrophilic part. So even when the cationic surfactants are dissolved in water, the hydrophilic part is directed to the water phase and the other hydrophobic part of the surfactant is located on the surface to decrease the force generated from the water phase. Increasing the surfactants' concentration reduces the water surface tension values. The intercept of the two regions at low concentrations and at higher surfactant concentrations gave the critical micelle concentration (CMC) values.

Table 4 summarizes the values of the standard free energy of micellization (ΔG_{mic}°) and the standard free energy of adsorption (ΔG_{ads}°). The obtained results indicated that compound DTB has a stronger adsorption ability on the carbon steel surface and a lower micellization ability than does compound HTB, leading to high corrosion protection.

The standard free energy of micellization (ΔG_{mic}°) for the investigated surfactants was calculated according to the following equation:

$$\Delta G_{mic}^{\circ} = RT \ln \mathrm{CMC} \tag{7}$$

The free standard energy standard of adsorption (ΔG_{ads}°) for the synthesized surfactants was calculated from the equation:

$$\Delta G_{ads}^{\circ} = -RT \ln K_{ads} \tag{8}$$

where K_{ads} represents the value of the adsorption equilibrium constant. The obtained results indicated that compound DTB with a longer alkyl chain possesses a stronger adsorption affinity onto the carbon steel surface than does compound HTB with a shorter alkyl chain, and this is leading to a higher inhibition efficiency.[36]

It is clear that the obtained data listed in Table 4 are in good agreement with the results obtained from both the potentiodynamic polarization and the electrochemical impedance spectroscopy techniques.

2.5. Molecular Modeling. The undertaken surfactants have a high adsorption affinity on the CS surface because of the presence of hetero atoms (N and S) in their chemical structures. DFT analysis can show the distribution of electron density over the molecular structure of the compounds.

The most important indices in the calculation of the important parameters according to eqs 9−11 are the energy of the highest full-field molecular orbital (E_H) and the energy of the lowest empty molecular orbital (E_L).

$$\Delta E_{gap} = E_L - E_H \tag{9}$$

$$\eta = \frac{\Delta E_{gap}}{2} \tag{10}$$

$$\sigma = \frac{1}{\eta} \tag{11}$$

The absolute electronegativity and hardness (Fe) of iron metal were chosen to be 0 eV and 0.[37] The Fe (110) plan work function is 4.82 eV (Fe). The 3d orbital of iron, as well as the donor−acceptor interaction between DTB and HTB, are responsible for facilitating adsorption. With increasing E_H values, electron donation from DTB and HTB into the vacant 3d iron orbital is enhanced.[38] DTB and HTB are more capable than E_L of acquiring electrons from the full-field 3d iron orbital. As shown in Figure 8, the electron density for HOMO in the gas phase is distributed over quaternary nitrogen and halogen atoms, whereas the electron cloud in the solution phase is distributed over the hetero and aromatic moieties and the halogenated groups. LUMO electrons are distributed over the same HOMO centers in both the gas and the solvated phases. Both HOMO's and LUMO's are thought to be hubs of donor−acceptor interactions.[39] Figure 8 depicts their alkyl chains using an electrostatic potential map that depicts the electron cloud distribution. This demonstrates that DTB and HTB have a proclivity to form a denser and stickier adsorption film.

Table 5 shows that the gas-phase N values are less than 3.6. DTB and HTB are electron donors that move electrons from metal surface to metal surface. The back-donation energy ($E_{back\text{-}donat}$) in Table 5 indicates that electrons from full-filled 3d or 4S orbitals of Fe are transferred to the LUMO of DTB and HTB. The donation and back-donation processes confirm the compound adsorption activity.[40]

https://doi.org/10.1021/acsomega.2c02961
ACS Omega 2022, 7, 32014−32025

Table 7. Data of Physical Investigation and Chemical Analysis of Formation Water Used in This Work

Physical Investigation			
total dissolved solids (T.D.S.)	9650 mg/L	density at 60 F	1.06 g/mL
salinity (as NaCl)	95556 mg/L	specific gravity	1.06
alkalinity (as $CaCO_3$)	320 mg/L	pH at 25 °C	6.8
total hardness (as $CaCO_3$)	14455 mg/L	conductivity	12.02×10^{-2} Ω/cm at 21.6 °C
		resistivity	0.0832 Ω m at 21.6 °C

Chemical Analysis					
cation	concn, mg/L	mequiv/L	anion	concn, mg/L	mequiv/L
Li^+	48.9	7.056	F^-	76.71	4.038
Na^+	30760.9	1337.485	Cl^-	57912.87	1631.405
NH_4^+	186.85	10.357	Br^-	252.62	3.163
K^+	945.24	24.179	NO_3^-	38.17	0.616
Mg^{2+}	947.95	78.007	NO_2	1.84	0.040
Sr^{2+}	4225.67	210.861	PO_4^{3-}	nil	nil
Ba^{2+}	78.08	1.783	SO_4^{2-}	640.54	13.342
Fe^{2+}	1.30	0.019	S^{2-}	325	0.020
Cu^{2+}	nil	nil	CO_3^{2-}	nil	nil
			HCO_3^-	390.40	6.399

2.6. Monte Carlo Simulation (MCs). DTB and HTB molecules are aligned in these images (Figure 9) in a way that is best suited to the most stable plane of Fe crystals (110). The MCs process can be used to mimic the adsorption properties of DTB and HTB on a CS surface. Because of the flat and planar orientation positions of the DTB and HTB optimized structures in the gas and solvent phases over Fe (110),[41] the adsorption process (donor−acceptor interactions) is efficiently carried out, as shown in the side and top views of Figure 9. The data in Table 7 show that DTB and HTB have a strong spontaneous adsorption affinity over the CS surface, resulting in large negative values of adsorption energy (E_{ads}) in the gas or solvated phases. It is worth noting that the value of E_{ads} in the solvent phase is greater than the equivalent in the gas phase. This is due to the formation of H-bonds between water solvent molecules and the nitrogen or/and oxygen atoms of DTB and HTB, which synergistically adsorb DTB and HTB to the CS surface. This is because the E_{ads} value of DTB and HTB is greater than the value of water. DTB and HTB have been shown to be capable of forming a protective adsorption barrier film on the CS surface.[42] Laboratory data (gravimetric and electrochemical) agree with the interpretations of the DFT and MCs output indices.

The data in Table 6 show that DTB and HTB have a strong spontaneous adsorption affinity over the CS surface, resulting in large negative values of adsorption energy (E_{ads}) in the gas or solvated phases. It is worth noting that the value of E_{ads} in the solvent phase is greater than the equivalent in the gas phase. The H-bond formed between the water solvent molecules and the nitrogen or/and oxygen atoms in the compound facilitates DTB adsorption on the CS surface. This demonstrates that compounds are capable of replacing water molecules adsorbing onto the CS surface and forming a protective adsorption barrier film.

2.7. Mechanism of the Corrosion Inhibition Process. The adsorption process of organic inhibitor molecules depends on many physical and chemical properties such as electron density, chemical structure, metal nature, charges at the metal/solution interface, and the type of aggressive medium (pH and/or electrode potential).

These properties affect the mode in which the molecules interact on the metal surface. Adsorption of organic molecules on solid surfaces cannot be considered purely physical or chemical; a combination of both processes can occur in adsorption.[43−45] Physical interaction is accepted as the first step for the adsorption of molecules on the metal surface, and then chemical adsorption may occur via different charge-sharing processes.[46] In a solution of oil field formation water, the inhibitor molecules are adsorbed on the metal surface through the following interactions: (i) the electrostatic

Scheme 1. Synthesis of Cationic Surfactants (DTB and HTB)

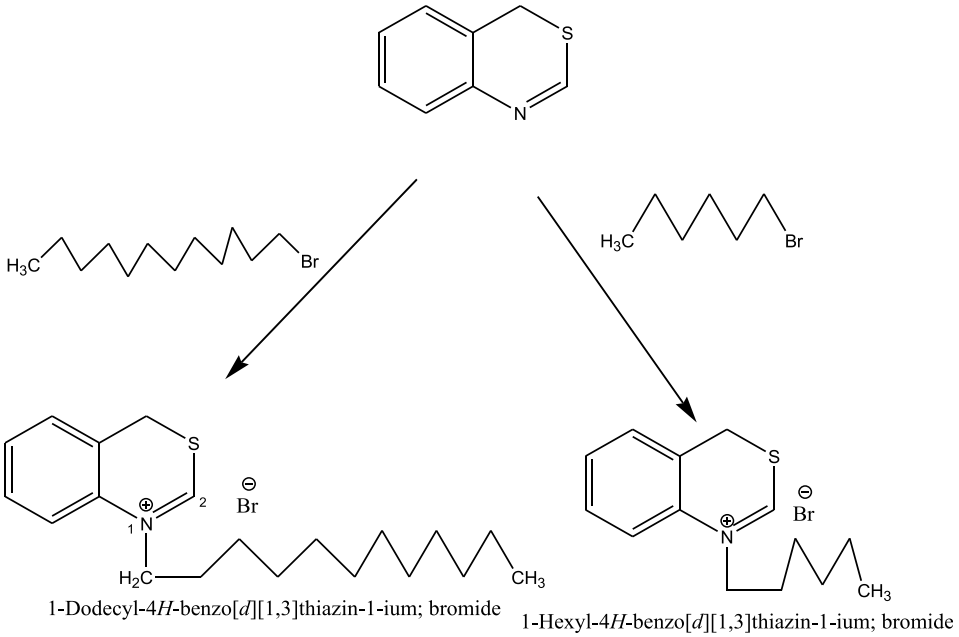

1-Dodecyl-4*H*-benzo[*d*][1,3]thiazin-1-ium; bromide

1-Hexyl-4*H*-benzo[*d*][1,3]thiazin-1-ium; bromide

https://doi.org/10.1021/acsomega.2c02961
ACS Omega 2022, 7, 32014−32025

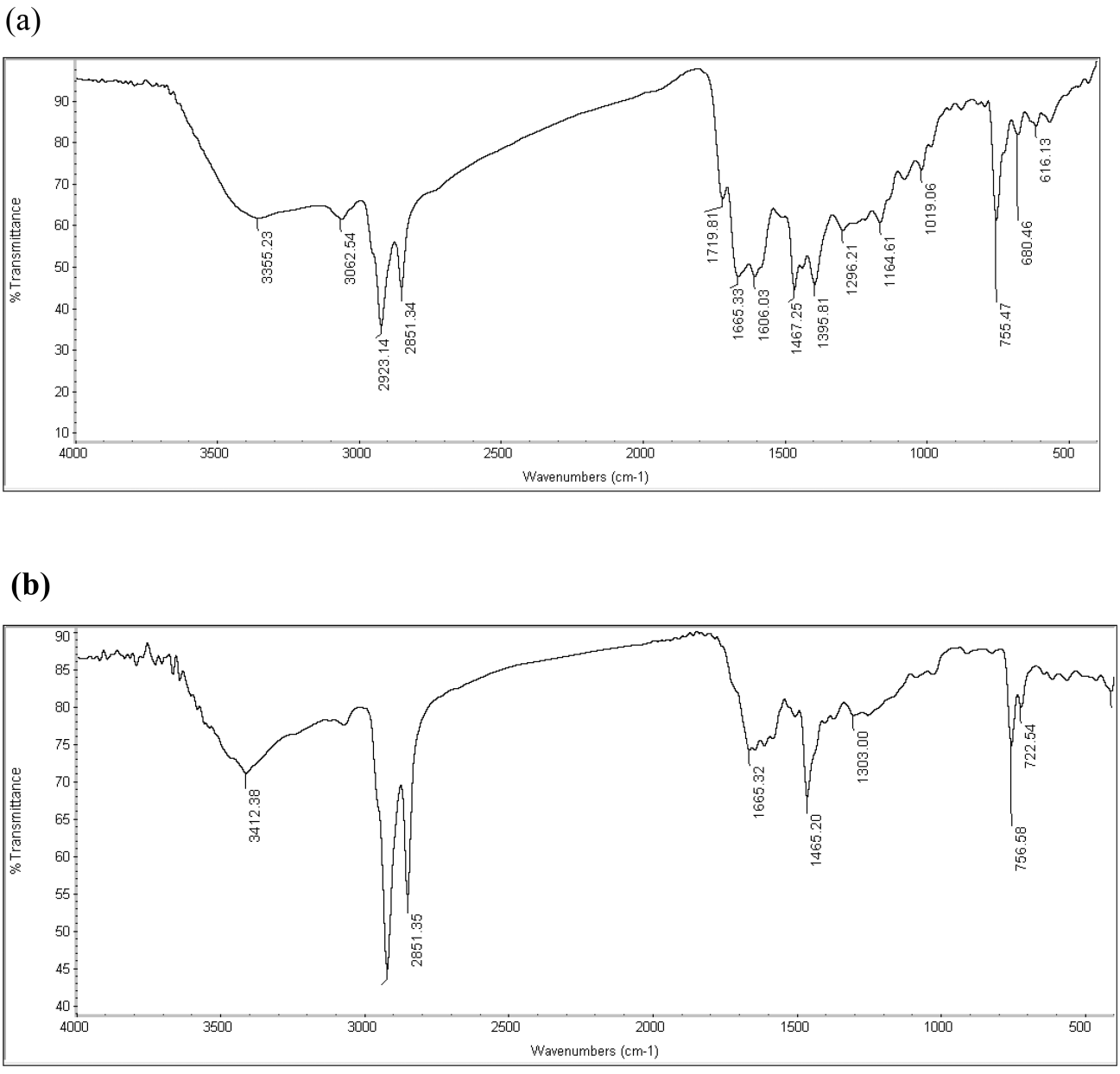

Figure 11. (a,b) FTIR spectrum of the synthesized inhibitors: (a) DTB and (b) HTB.

interaction between the positively protonated inhibitor and the chloride ions adsorbed on the carbon steel surface (physisorption process); (ii) the chemical interaction between the lone-pair electrons on the heteroatoms (N, S, and O) and the unoccupied d-orbital on the Fe surface (chemical adsorption process); and (iii) the donor−acceptor interaction between the π-electrons of the aromatic ring and the vacant d-orbitals on the metal surface. The presence of electron donation increases the electron density of the neighboring aromatic ring and makes the π-electrons more available for interaction with the C-steel surface, and thus strengthens the adsorption of the alkyl chain on the steel surface. A skeletal representative of the mode of adsorption of compound DTB is shown in Figure 10.

It is well-known that as the alkyl chain length increases, the hydrophobicity of the compound increases, in addition to the increase in the minimum area per molecule A_{min}. This leads to an increase in the strength of the protective layer that isolates the surface from the environment and increases the inhibition efficiencies as well as the adsorption process.[47]

3. EXPERIMENTAL SECTION

3.1. Components of API5L X-65 Type Carbon Steel Alloy. Carbon steel samples were cut from an unused oil pipeline for this study (Belayim Petroleum Co., Egypt). The chemical composition (wt %) of carbon steel is C, 0.09; Si, 0.22; Mn, 1.52; P, 0.01; S, 0.05; Ni, 0.04; Cr, 0.02; Mo, 0.004; V, 0.002; Cu, 0.02; Al, 0.04, and the reset is Fe.

3.2. Deep Oil Wells' Formation Water. Deep oil wells' formation water naturally exists in the reservoir rocks before drilling. The chemical composition and physical features of the oil well formation water studied are shown in Table 7.

3.3. Testing Solution. The testing solution of this study is oil well formation water with the above-mentioned chemical composition. The reaction of sodium sulfide (3.53 mg L^{-1}) with acetic acid (1.7 mg L^{-1}) generates H_2S gas.

https://doi.org/10.1021/acsomega.2c02961
ACS Omega 2022, 7, 32014−32025

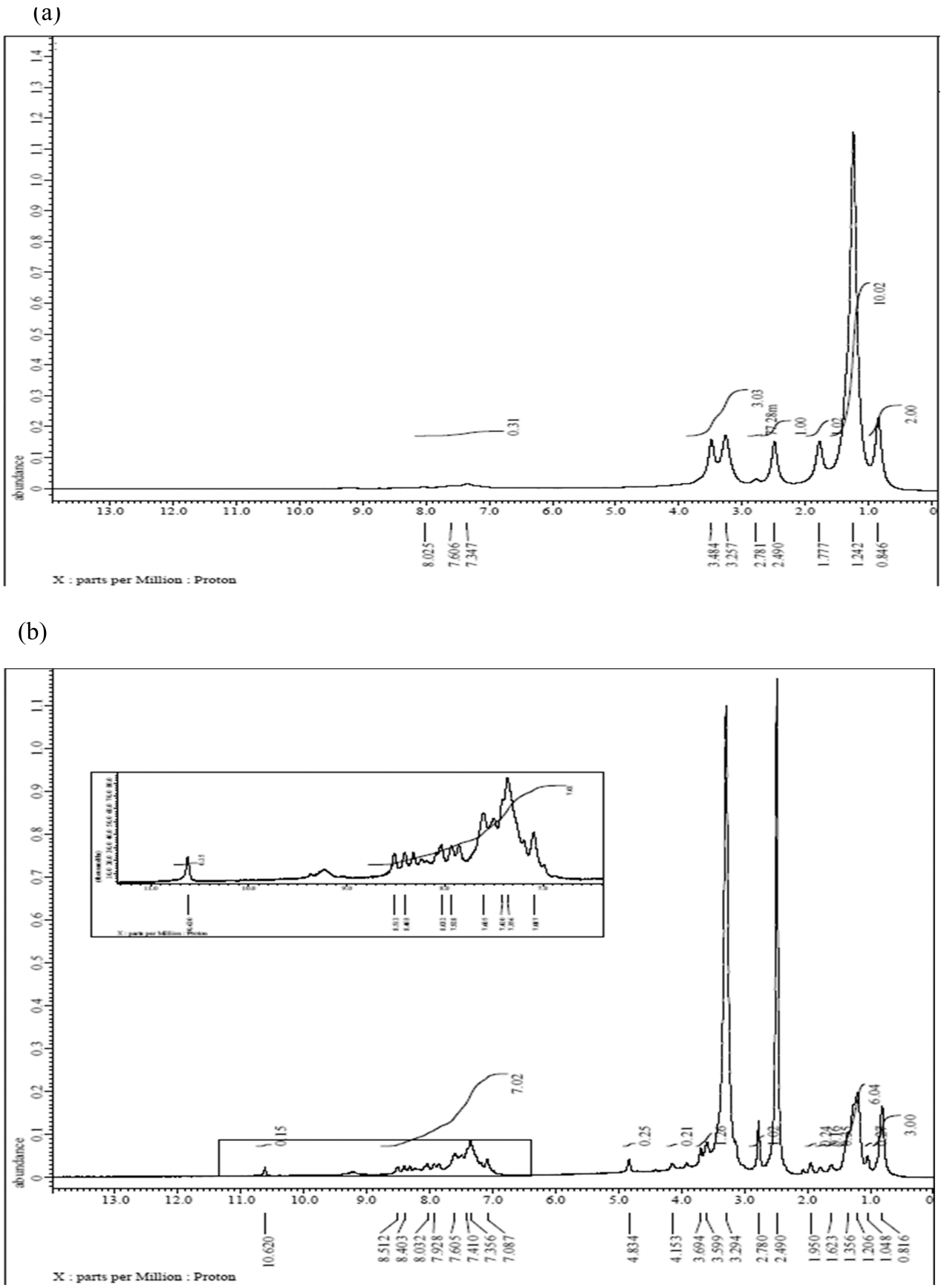

Figure 12. Nuclear magnetic resonance spectroscopy of the inhibitor: (a) ^{1}H NMR of DTB and (b) ^{1}H NMR of HTB.

https://doi.org/10.1021/acsomega.2c02961
ACS Omega 2022, 7, 32014−32025

3.4. Synthesis of the Inhibitors. Scheme 1 shows the synthesis of the benzothiazole-based cationic surfactant DTB. To perform this procedure, the quaternization reaction was used. In a 250 mL round flask were charged 50 mM benzothiazole and 50 mM 1-bromooctadecane separately, in the presence of acetone (100 mL) as a solvent. The reaction mixture was refluxed under stirring for 18 h and cooled to room temperature. The obtained brown precipitate was filtered, washed twice with diethyl ether, and then recrystallized from acetone to afford the white crystal products of the cationic surfactants. The yields of the brown crystal product ranged between 78% and 86%.

Hexyl bromide-based cationic surfactant HTB was produced as depicted in Scheme 1. The quaternization reaction was used to perform this task using the same procedures as previously mentioned. The yield of the brown crystal products ranged between 80% and 90%.

3.4.1. Data of FTIR. The FTIR spectrum (Figure 11) of the prepared inhibitors (DTB, HTB) shows two peaks at 3355 and 3412 cm^{-1} ascribed to N−H in both inhibitors, 2923 and 2851 cm^{-1} corresponding to CH_3 and CH_2, in addition to the peak at 1065 cm^{-1} and the fingerprint peak at 722 cm^{-1} that referred to the asymmetric and symmetric stretching quaternary nitrogen atom (N^+−C) as shown in Figure 11a,b.

3.4.2. ^1H NMR Spectrum Spectroscopic Analysis. Figure 12a,b shows the substance shift at δ (0.96) for ^1H proton (a) $-CH_3$, the substance shift δ (4.13) for ^1H proton (b), and the chemical shifts between δ (7.2) for ^1H protons (g) and (h) of the benzene ring. All of these chemical reactions prove that compound DTB was properly synthesized. The chemical shifts that obviously appeared in the ^1H NMR spectrum were regarded as strong evidence that compound HTB was successfully prepared. The obtained surfactant possesses a hydrogen proton distribution that is consistent with its predicted structure in Figure 12a,b.

3.5. Electrochemical Measurements. *3.5.1. Potentiodynamic Polarization Measurement.* To determine potentiodynamic polarization, we used an e-glass cell with a working electrode of 1 cm^2 surface area and two other electrodes: a platinum reference electrode and a SCE saturated with water. A potentiostat type (Tacussel-radiometer PGZ402) and corrosion analysis software model PGZ402 were used. The scan rate was 1 mV s^{-1} after immersion of the three electrodes into the test solution for 60 min to obtain the steady-state potential in the absence and presence of a certain inhibitor concentration.

3.5.2. Electrochemical Impedance Spectroscopy (EIS). We performed EIS on the same electrochemical cell at an OCP amplitude of 10 mV between the frequencies of 100 kHz and 20 mHz.

3.6. Surface Tension Measurements. For varied concentrations of the examined surfactants, the surface tension was measured with a Kruss K6 tensiometer, a direct surface tension measurement utilizing the ring method.

3.7. Surface Examination. After 12 days in the test solution, the intended samples were withdrawn, cleaned, rinsed, and dried with distilled water before being analyzed using SEM.

3.8. Quantum Calculation Details. In this work, quantum chemical calculations were carried out by using *Gaussian 09W* software, with a neutral and cationic LP (LP, LPH+)+G(d, p) basis set at the DFT level. The corresponding quantum chemical parameters were obtained and discussed in detail. Moreover, a study on the adsorption mode and the corresponding bonding strength of the inhibitor molecules on a metal surface is indispensable to understand its inhibitive performance. The interaction between the inhibitor molecules and steel surface was highlighted using a molecular mechanics method as implemented in the Forcite module. A simulation box of 24.3 × 17.2 × 67.1 Å dimension containing 5 layers of Fe (110), 1 inhibitor molecule, 500 H_2O molecules, and a 40 Å vacuum layer was established. The periodic boundary condition and the COMPASS force field were used in this system. A fine quality simulation was accomplished with a 500 ps simulation time and a 1 fs time step using the NVT canonical ensemble.

4. CONCLUSIONS

In deep oil well formation water, surfactants DTB and HTB are effective inhibitors of the breakdown of carbon steel. The structure of the surfactants was confirmed by FTIR and nuclear magnetic resonance ^1H NMR spectroscopic techniques. The obtained polarization data confirmed that the selected cationic surfactants act as mixed-type inhibitors, but the anodic effect was predominant. As seen in SEM micrographs, the corrosion-resistant environment was effectively isolated from the surface. How the synthesized surfactants performed as corrosion inhibitors was increased with increasing concentration until the CMC was reached. Also, E_{HOMO} and the ΔN parameters are further proof of the inhibition effect of the used surfactants. Finally, the Monte Carlo simulation approach confirmed the correlation between both the experimental and the theoretical results.

AUTHOR INFORMATION

Corresponding Author

Elsayed Gamal Zaki − *Egyptian Petroleum Research Institute, Nasr City, Cairo 11727, Egypt;* orcid.org/0000-0001-7053-3169; Email: chemparadise17@yahoo.com

Authors

Mohamed A. Moselhy − *Belayim Petroleum Company, Cairo 7074, Egypt*

Samir Abd El Hady Abd El-Maksoud − *Chemistry Department, Faculty of Science, Port Said University, Port Said 42522, Egypt*

Mohamed A. Migahed − *Egyptian Petroleum Research Institute, Nasr City, Cairo 11727, Egypt*

Complete contact information is available at: https://pubs.acs.org/10.1021/acsomega.2c02961

Notes

The authors declare no competing financial interest.

REFERENCES

(1) Ghareba, S.; Omanovic, S. Interaction of 12-aminododecanoic acid with a carbon steel surface: towards the development of 'green' corrosion inhibitors. *Corros. Sci.* **2010**, *52*, 2104−2113.

(2) Shaban, M. M.; Negm, N. A.; Farag, R. K.; Fadda, A. A.; Gomaa, A. E.; Farag, A. A.; Migahed, M. A. Anti-corrosion, antiscalant and anti-microbial performance of some synthesized trimeric cationic imidazolium salts in oilfield applications. *J. Mol. Liq.* **2022**, *351*, 118610.

(3) Hernández-Espejel, A.; Dominguez-Crespo, M. A.; Cabrera-Sierra, R.; Rodríguez-Meneses, C.; Arce-Estrada, E. M. Investigations of corrosion films formed on API-X52 pipeline steel in acid sour media. *Corros. Sci.* **2010**, *52*, 2258−2267.

https://doi.org/10.1021/acsomega.2c02961
ACS Omega 2022, 7, 32014−32025

(4) Migahed, M. A.; Zaki, E. G.; Shaban, M. M. Corrosion control in the tubing steel of oil wells during matrix acidizing operations. *RSC adva.* **2016**, *6*, 71384−71396.
(5) Galai, M.; Rbaa, M.; Serrar, H.; Ouakki, M.; Ech-chebab, A.; Abousalem, A. S.; Ech-chihbi, E.; Dahmani, K.; Boukhris, S.; Zarrouk, A.; EbnTouhami, M. S-Thiazine as effective inhibitor of mild steel corrosion in HCl solution: Synthesis, experimental, theoretical and surface assessment. *Colloids Surf., A* **2021**, *613*, 126127.
(6) Kannan, P.; Varghese, A.; Palanisamy, K.; Abousalem, A. S.; George, L. (2020). Evaluation of corrosion mitigation performance of 1-(3, 4, 5-trimethoxyphenylmethylidene)-2-naphthylamine (TMPNA) Schiff's base on carbon steel using electrochemical, thermodynamic and theoretical approaches. *J. Bio. Tribo. Corros.* **2020**, *6* (4), 1−17.
(7) Prabakaran, M.; Kim, S. H.; Hemapriya, V.; Chung, I. M. Evaluation of polyphenol composition and anti-corrosion properties of Cryptostegia grandiflora plant extract on mild steel in acidic medium. *J. Ind. Eng. Chem.* **2016**, *37*, 47−56.
(8) Fouda, A. S.; Abd El-Maksoud, S. A.; El-Habab, A. T.; Ibrahim, A. R. Synthesis and characterization of novel fatty alcohol ethoxylate surfactants for corrosion inhibition of mild steel. *J. Bio. Tribo. Corros.* **2021**, *7* (1), 1−14.
(9) Murira, C. M.; Punckt, C.; Schniepp, H. C.; Khusid, B.; Aksay, I. A. Inhibition and promotion of copper corrosion by CTAB in a microreactor system. *Langmuir* **2008**, *24*, 14269−14275.
(10) Kumar, A. Corrosion inhibition of mild steel in hydrochloric acid by Sodium Lauryl Sulfate (SLS). *E-J. Chem.* **2008**, *5* (2), 275−280.
(11) El-Monem, M. A.; Shaban, M. M.; Migahed, M. A.; Khalil, M. M. Synthesis, Characterization, and Computational Chemical Study of Aliphatic Tricationic Surfactants as Corrosion Inhibitors for Metallic Equipment in Oil Fields. *ACS omega* **2020**, *5*, 26626−26639.
(12) Pinazo, A.; Manresa, M. A.; Marques, A. M.; Bustelo, M.; Espuny, M. J.; Pérez, L. Amino acid−based surfactants: New antimicrobial agents. *Adv. Colloid Interface Sci.* **2016**, *228*, 17−39.
(13) Abdrabo, W. S.; Elgendy, B.; Soliman, K. A.; Abd El-Lateef, H. M.; Tantawy, A. H. Synthesis, assessment and corrosion protection investigations of some novel peptidomimetic cationic surfactants: Empirical and theoretical insights. *J. Mol. Liq.* **2020**, *315*, 113672.
(14) Farag, A. A.; Eid, A. M.; Shaban, M. M.; Mohamed, E. A.; Raju, G. Integrated modeling, surface, electrochemical, and biocidal investigations of novel benzothiazoles as corrosion inhibitors for shale formation well stimulation. *J. Mol. Liq.* **2021**, *336*, 116315.
(15) Shalabi, K.; Helmy, A. M.; El-Askalany, A. H.; Shahba, M. M. New pyridinium bromide mono-cationic surfactant as corrosion inhibitor for carbon steel during chemical cleaning: Experimental and theoretical studies. *J. Mol. Liq.* **2019**, *293*, 111480.
(16) Gao, M.; Zhang, J.; Liu, Q.; Li, J.; Zhang, R.; Chen, G. Effect of the alkyl chain of quaternary ammonium cationic surfactants on corrosion inhibition in hydrochloric acid solution. *Comptes Rendus Chimie* **2019**, *22*, 355−362.
(17) Hegazy, A. Y.; El-Shafaie, M.; Berry, K. M. Novel cationic surfactants for corrosion inhibition of carbon steel pipelines in oil and gas wells applications. *J. Mol. Liq.* **2016**, *214*, 347−356.
(18) Hegazy, M. A.; Abd El Rehim, S. S.; Badawi, A. M.; Ahmed, M. Y. Studying the corrosion inhibition of carbon steel in hydrochloric acid solution by 1-dodecyl-methyl-1 H-benzo [d][1, 2, 3] triazole-1-ium bromide. *RSC Adv.* **2015**, *5*, 49070−49079.
(19) Migahed, M. A.; Aly, R. O.; Al-Sabagh, A. M. Impact of gamma-ray-pre-irradiation on the efficiency of corrosion inhibition of some novel polymeric surfactants. *Corros. Sci.* **2004**, *46*, 2503−2516.
(20) Migahed, M. A.; Attia, A. A.; Habib, R. E. (2015). Study on the efficiency of some amine derivatives as corrosion and scale inhibitors in cooling water systems. *RSC adv.* **2015**, *5*, 57254−57262.
(21) Caporali, S.; Fossati, A.; Lavacchi, A.; Perissi, I.; Tolstogouzov, A.; Bardi, U. Aluminium electroplated from ionic liquids as protective coating against steel corrosion. *Corros. Sci.* **2008**, *50*, 534−539.
(22) Yue, G.; Lu, X.; Zhu, Y.; Zhang, X.; Zhang, S. (2009). Surface morphology, crystal structure and orientation of aluminium coatings electrodeposited on mild steel in ionic liquid. *Chem. Eng. J.* **2009**, *147*, 79−86.
(23) Migahed, M. A.; Farag, A. A.; Elsaed, S. M.; Kamal, R.; El-Bary, H. A. Corrosion inhibition of steel pipelines in oil well formation water by a new family of nonionic surfactants. *Chem. Eng. Commun.* **2012**, *199*, 1335−1356.
(24) Zhao, P.; Zhong, C.; Hunag, L.; Niu, L.; Zhang, F. Corrosion inhibition of dibenzo [1, 4, 8, 11] tetraaza [14] annulene nickel on steel in 1 M HCl. *Corros. Sci.* **2008**, *50*, 2166−2171.
(25) Kimizuka, N.; Nakashima, T. Spontaneous self-assembly of glycolipid bilayer membranes in sugar-philic ionic liquids and formation of ionogels. *Langmuir* **2001**, *17*, 6759−6761.
(26) Shaban, M. M.; Eid, A. M.; Farag, R. K.; Negm, N. A.; Fadda, A. A.; Migahed, M. A. Novel trimeric cationic pyrdinium surfactants as bi-functional corrosion inhibitors and antiscalants for API 5L X70 carbon steel against oilfield formation water. *J. Mol. Liq.* **2020**, *305*, 112817.
(27) Pernak, J.; Sobaszkiewicz, K.; Foksowicz-Flaczyk, J. Ionic liquids with symmetrical dialkoxymethyl-substituted imidazolium cations. *Chemistry−A European Journal* **2004**, *10*, 3479−3485.
(28) Abdel-Rahman, L. H.; Adam, M. S. S.; Abu-Dief, A. M.; Moustafa, H.; Basha, M. T.; Aboraia, A. S.; Al-Farhan, B. S. Synthesis, theoretical investigations, biocidal screening, DNA binding, in vitro cytotoxicity and molecular docking of novel Cu (II), Pd (II) and Ag (I) complexes of chlorobenzylidene Schiff base: Promising antibiotic and anticancer agents. *Appl. Organomet. Chem.* **2018**, *32*, e4527.
(29) Oguzie, E. E.; Enenebeaku, C. K.; Akalezi, C. O.; Okoro, S. C.; Ayuk, A. A.; Ejike, E. N. Adsorption and corrosion-inhibiting effect of Dacryodis edulis extract on low-carbon-steel corrosion in acidic media. *J. Colloid interface Sci.* **2010**, *349*, 283−292.
(30) Musa, A. Y.; Kadhum, A. A. H.; Mohamad, A. B.; Takriff, M. S. Molecular dynamics and quantum chemical calculation studies on 4, 4-dimethyl-3-thiosemicarbazide as corrosion inhibitor in 2.5 M H_2SO_4. *Mater. Chem. Phys.* **2011**, *129*, 660−665.
(31) Ju, H.; Kai, Z. P.; Li, Y. Aminic nitrogen-bearing polydentate Schiff base compounds as corrosion inhibitors for iron in acidic media: a quantum chemical calculation. *Corros. Sci.* **2008**, *50*, 865−871.
(32) Singh, P.; Ebenso, E. E.; Olasunkanmi, L. O.; Obot, I. B.; Quraishi, M. A. Electrochemical, theoretical, and surface morphological studies of corrosion inhibition effect of green naphthyridine derivatives on mild steel in hydrochloric acid. *J. Phys. Chem. C* **2016**, *120*, 3408−3419.
(33) Rahmati, M.; Modarress, H. Nitrogen adsorption on nanoporous zeolites studied by Grand Canonical Monte Carlo simulation. *J. Mol. Struct. THEOCHEM* **2009**, *901*, 110−116.
(34) Zhang, Z.; Tian, N. C.; Huang, X. D.; Shang, W.; Wu, L. Synergistic inhibition of carbon steel corrosion in 0.5 M HCl solution by indigo carmine and some cationic organic compounds: experimental and theoretical studies. *RSC adv.* **2016**, *6*, 22250−22268.
(35) Hu, Z.; Meng, Y.; Ma, X.; Zhu, H.; Li, J.; Li, C.; Cao, D. Experimental and theoretical studies of benzothiazole derivatives as corrosion inhibitors for carbon steel in 1 M HCl. *Corros. Sci.* **2016**, *112*, 563−575.
(36) Umoren, S. A.; Ebenso, E. E. (2007). The synergistic effect of polyacrylamide and iodide ions on the corrosion inhibition of mild steel in H_2SO_4. *Mater. Chem. Phys.* **2007**, *106*, 387−393.
(37) Olasunkanmi, L. O.; Idris, A. O.; Adewole, A. H.; Wahab, O. O.; Ebenso, E. E. Adsorption and Corrosion Inhibition Potentials of Salicylaldehyde-based Schiff Bases of Semicarbazide and p-Toluidine on Mild Steel in Acidic Medium: Experimental and Computational Studies. *Surf. Interfaces* **2020**, *21*, 100782.
(38) Verma, C.; Quraishi, M. A.; Singh, A. 2-Amino-5-nitro-4, 6-diarylcyclohex-1-ene-1, 3, 3-tricarbonitriles as new and effective corrosion inhibitors for mild steel in 1 M HCl: Experimental and theoretical studies. *J. Mol. Liq.* **2015**, *212*, 804−812.
(39) Zhang, Z.; Li, W.; Zhang, W.; Huang, X.; Ruan, L.; Wu, L. Experimental, quantum chemical calculations and molecular dynamics

https://doi.org/10.1021/acsomega.2c02961
ACS Omega 2022, 7, 32014−32025

(MD) simulation studies of methionine and valine as corrosion inhibitors on carbon steel in phase change materials (PCMs) solution. *J. Mol. Liq.* **2018**, *272*, 528−538.
(40) Obot, I. B.; Ebenso, E. E.; Kabanda, M. M. Metronidazole as environmentally safe corrosion inhibitor for mild steel in 0.5 M HCl: experimental and theoretical investigation. *J. Environ. Chem. Eng.* **2013**, *1*, 431−439.
(41) Jmiai, A.; Tara, A.; El Issami, S.; Hilali, M.; Jbara, O.; Bazzi, L. A new trend in corrosion protection of copper in acidic medium by using Jujube shell extract as an effective green and environmentally safe corrosion inhibitor: Experimental, quantum chemistry approach and Monte Carlo simulation study. *J. Mol. Liq.* **2021**, *322*, 114509.
(42) Elgendy, A.; Elkholy, A. E.; El Basiony, N. M.; Migahed, M. A. Monte Carlo simulation for the antiscaling performance of Gemini ionic liquids. *J. Mol. Liq.* **2019**, *285*, 408−415.
(43) Ismail, M. A.; Shaban, M. M.; Abdel-Latif, E.; Abdelhamed, F. H.; Migahed, M. A.; El-Haddad, M. N.; Abousalem, A. S. Novel cationic aryl bithiophene/terthiophene derivatives as corrosion inhibitors by chemical, electrochemical and surface investigations. *Sci. Rep.* **2022**, *12*, 1−16.
(44) Negm, N. A.; Migahed, M. A.; Farag, R. K.; Fadda, A. A.; Awad, M. K.; Shaban, M. M. High performance corrosion inhibition of novel tricationic surfactants on carbon steel in formation water: Electrochemical and computational evaluations. *J. Mol. Liq.* **2018**, *262*, 363−375.
(45) Galai, M.; Rbaa, M.; Ouakki, M.; Abousalem, A. S.; Ech-Chihbi, E.; Dahmani, K.; Dkhireche, N.; Lakhrissi, B.; EbnTouhami, M. Chemically functionalized of 8-hydroxyquinoline derivatives as efficient corrosion inhibition for steel in 1.0 M HCl solution: Experimental and theoretical studies. *Surf. Interfaces* **2020**, *21*, 100695.
(46) Umoren, S. A.; Obot, I. B.; Ebenso, E. E. Corrosion inhibition of aluminium using exudate gum from Pachylobus edulis in the presence of halide ions in HCl. *E-journal Chem.* **2008**, *5*, 355−364.
(47) Ahamad, I.; Prasad, R.; Quraishi, M. A. Adsorption and inhibitive properties of some new Mannich bases of Isatin derivatives on corrosion of mild steel in acidic media. *Corros. Sci.* **2010**, *52*, 1472−1481.

https://doi.org/10.1021/acsomega.2c02961
ACS Omega 2022, 7, 32014−32025